Journal of Sound and Vibration 595 (2025) 118711

Contents lists available at ScienceDirect

Journal of Sound and Vibration

journal homepage: www.elsevier.com/locate/jsvi

Acoustic capsule: A structure that can carry different objects but obtain the same acoustic radiation force

Menyang Gong [a,b], Yuanyuan Li [a], Yupei Qiao [c], Xin Xu [a], Zhonghan Fei [a], Shenlian Gao [a], Jiehui Liu [a], Aijun He [d,*], Xiaozhou Liu [a,e,**]

[a] Key Laboratory of Modern Acoustics, Institute of Acoustics and School of Physics, Collaborative Innovation Center of Advanced Microstructures, Nanjing University, Nanjing 210093, China
[b] School of Electronic and Information Engineering, Nanjing University of Information Science and Technology, Nanjing 210044, China
[c] School of Physics and Electronic Science, Guizhou Normal University, Guiyang 550001, China
[d] School of Electronic Science and Engineering, Nanjing University, Nanjing 210023, China
[e] State Key Laboratory of Acoustics, Institute of Acoustics, Chinese Academy of Sciences, Beijing 100190, China

ARTICLE INFO

Keywords:
Acoustic manipulation
Acoustic radiation force
Acoustic tweezers

ABSTRACT

An acoustic capsule is designed utilizing equivalent anisotropy of density and of sound speed. The designed capsule can carry any object with dimensions smaller than those of its inner cavity. The capsule achieves internal shielding of the sound field, thus ensuring that the capsule and its contents experience the same acoustic radiation force (ARF), regardless of any changes in the contents. An acoustic capsule design method is proposed and its feasibility is verified using a combination of theoretical analysis and finite element simulations. Additionally, optimization strategies to enhance the ARF and enable selection of appropriate material parameters are discussed, and these strategies pave the way toward practical applications of the ARF in life sciences and other fields.

1. Introduction

The discovery of optical tweezers, which earned the Nobel Prize in Physics in 2018, has led to significantly heightened interest in particle manipulation using the nonlinearity of beams [1–11]. When compared with the optical radiation force, use of the acoustic radiation force (ARF) for particle manipulation offers several distinct advantages, including improved biocompatibility, reduced thermal effects, and greater penetrability. Additionally, the wavelengths that are commonly used for ARF generation are particularly well-suited to manipulating cells and tissues within fluidic environments [12–19]. These attributes underline the broad potential of ARF-based particle manipulation techniques for applications in life sciences and medicine. In a pioneering work in 1905, Rayleigh calculated the ARF acting on a rigid plate in a plane wave sound field within an ideal fluid, thus providing the first theoretical explanation and first definition of the ARF [20]. Subsequently, theoretical solutions were developed for commonly encountered ARFs using spherical and cylindrical particles [21–31]. Mitri's in-depth investigation of the calculation solutions for the ARFs experienced by multilayer shells in various media under the influence of a diverse range of incident waves represents a significant milestone in the exploration of the ARF on multilayered structures and has provided valuable insights for subsequent research efforts within this domain [32–42]. Recent studies of the scattering characteristics of multilayered spherical encapsulants have provided

* Corresponding author.
** Corresponding author at: Key Laboratory of Modern Acoustics, Institute of Acoustics and School of Physics, Collaborative Innovation Center of Advanced Microstructures, Nanjing University, Nanjing 210093, China.
E-mail addresses: haj@nju.edu.cn (A. He), xzliu@nju.edu.cn (X. Liu).

https://doi.org/10.1016/j.jsv.2024.118711
Received 15 June 2023; Received in revised form 30 August 2024; Accepted 30 August 2024
Available online 2 September 2024

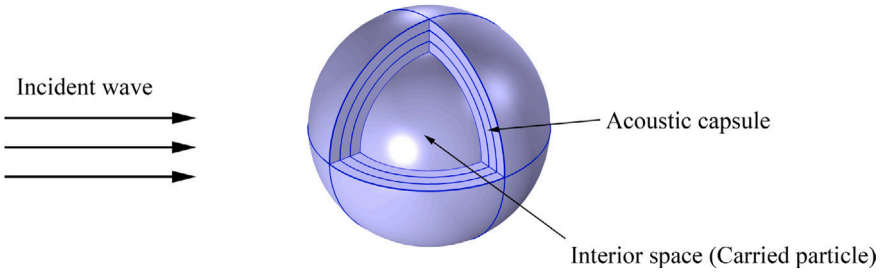

Fig. 1. Schematic diagram of an acoustic capsule with a multilayer structure imitation.

important guidelines for ARF calculations and additional material design considerations [43,44]. Furthermore, major advancements have been made in the acoustic microfluidics field based on acoustic manipulation, providing novel application scenarios for and insights into acoustic manipulation techniques [45–58]. Recently, there has also been a surge of interest in active steering or active acoustic carriers, which also represent novel avenues for use of acoustic manipulation techniques [59–64]. Active feedback through a piezoelectric drive can enable adaptive regulation of the geometric parameters of the structure to be controlled, which provides an ingenious concept for ARF transmission schemes. However, the cost of implementation of this active regulation method is high and its robustness is poor, which means that the use of passive solutions to achieve precise acoustic manipulation offers considerable research value.

Because of the sensitivity of the structural parameters and the frequency of the incident wave to the action of the ARF, transporting the ARF in different situations often necessitates the development of a new design based on new materials. Therefore, development of a controllable ARF transport solution that is not constrained by the parameters of the object to be transported has become a problem that urgently requires a solution. In medicine, various drugs are often delivered in the form of capsules, e.g., in starch capsules, to avoid stimulating the patient's stomach. This has led us to a similar concept: we can realize uniform and controllable transport of a variety of objects by designing an "acoustic capsule". In this work, the concept of the "acoustic capsule" is proposed, which represents an innovative approach to acoustic transmission in which the ARF can be tuned through appropriate design of the transmission structure. An acoustic capsule functions in a manner similar to a conventional capsule; it serves as a carrier that can accommodate contents while also preventing specific interactions between these contents and the external environment. Specifically, an acoustic capsule prevents acoustic interactions between its contents and the external environment, thus ensuring that the capsule and its contents experience the same ARF while the capsule accommodates various objects. In traditional multilayered spherical cavity structures, different objects will typically experience distinct ARFs.

The capsule must meet two requirements. First, the capsule should shield the inner cavity from the sound field, such that the ARF that acts on the capsule and its contents as a whole is not influenced by the contents. Second, the ARF received by the entire capsule and its contents should be maximized.

2. Theory: Construction of density anisotropy and calculation of the acoustic radiation force

The mechanical parameters of materials, such as the density, can be expanded into tensors, thus enabling the theoretical construction of anisotropic structures. In 1983, Schoenberg and Sen proposed a scheme to achieve anisotropy through use of layered periodic structures [65]. To ensure the universality of the proposed transport structure, the acoustic capsule should be a spherical shell; otherwise, the direction of the incident waves would be severely limited. Therefore, the actual acoustic capsule structure, as depicted in Fig. 1, consists of a multilayered spherical shell encapsulant on the exterior with a carrying space in the interior that can hold any object. However, spherical structures cannot satisfy the long-range order requirements of crystals to achieve radial and transverse anisotropy, and thus it is necessary to realize the density anisotropy of multilayered homogeneous materials through acoustic series connections and parallel connections. This principle was also used for the famous acoustic cloak several years ago [66]. It is important to note here that where the acoustic cloak requires the equivalent parameters of the layered periodic structure to match those of the external medium to ensure invisibility, the acoustic capsule has no such requirement. Instead, the transport structure of the acoustic capsule must alter the external sound field to obtain the most appropriate ARF. The transport structure is allowed to modify the external sound field but it must also prevent the sound field from entering the carrying space. Essentially, from a mathematical perspective, this represents a relaxation of constraints.

Equivalent parameter methods have been validated widely and used extensively in the acoustic metamaterials field [65–71]. The single-layer thickness of the multilayered spherical shell structures adopted in this work is significantly smaller than the wavelength of the sound waves, thus allowing them to be regarded as acoustic metamaterials. Therefore, use of equivalent parameter methods in the analysis of the acoustic field is justifiable. The results of subsequent theoretical calculations and finite element simulations also support this view.

For periodic layered structures, when the wavelength of the sound wave is greater than the thickness of a single layer, an expression of the equivalent densities can be given as

$$\begin{aligned}\rho_r &= \frac{\Sigma_{n=1}^{m}\eta_n\rho_n}{\Sigma_{n=1}^{m}\eta_n},\\ \rho_\theta &= \frac{\Sigma_{n=1}^{m}\eta_n}{\Sigma_{n=1}^{m}\frac{\eta_n}{\rho_n}}.\end{aligned} \tag{1}$$

The bulk modulus can be expressed here as

$$\kappa = \frac{\Sigma_{n=1}^{m}\eta_n}{\Sigma_{n=1}^{m}\frac{\eta_n}{\kappa_n}}, \tag{2}$$

where m represents the number of layers of the material. The conversion relationship between the bulk modulus κ, the elastic modulus E, and Poisson's ratio μ can be expressed as follows:

$$\begin{aligned}\kappa &= \frac{E}{3(1-2\mu)},\\ d_p &: d_q = \eta_p : \eta_q,\end{aligned} \tag{3}$$

where ρ_r and ρ_θ are the radial and transverse components of the density of the equivalent material, ρ_n and η_n are the density and the relative thickness of the nth layer of the material, and d_p and d_q are the actual thicknesses of layer p and layer q, respectively; finally, κ is the bulk modulus of the equivalent material.

If the model is simplified into two types of layers, denoted by A and B, then we obtain

$$\begin{aligned}\rho_r &= \frac{\rho_A+\eta\rho_B}{1+\eta},\\ \frac{1}{\rho_\theta} &= \frac{1}{1+\eta}\left(\frac{1}{\rho_A}+\frac{\eta}{\rho_B}\right),\\ \frac{1}{\kappa} &= \frac{1}{1+\eta}\left(\frac{1}{\kappa_A}+\frac{\eta}{\kappa_B}\right),\\ \eta &= d_A/d_B,\end{aligned} \tag{4}$$

where d_A and d_B are the total thicknesses of materials A and B, and κ_A and κ_B are the bulk moduli of these two materials, respectively. Because the equations in Eq. (4) are indeterminate equations, the parameters A and B that constitute the capsule can have a large selection space. Any material can be selected as long as Eq. (4) is satisfied.

For the acoustic capsule, the equivalent parameters can be adjusted. If required, the equivalent structural parameters of ρ_{rw}, $\rho_{\theta w}$, and κ_{rw} can be adjusted as follows:

$$\begin{aligned}\frac{\rho_r}{\rho_{rw}} &= \frac{r}{r-a},\\ \frac{\rho_\theta}{\rho_{rw}} &= \frac{r-a}{r},\\ \frac{\kappa_{rw}}{\kappa} &= \left(\frac{b}{b-a}\right)^2\frac{r-a}{r},\end{aligned} \tag{5}$$

where a is the inner radius of the capsule, b is the outer radius of the capsule, and ρ_{rw}, $\rho_{\theta w}$, and κ_{rw} represent the radial component of the effective anisotropic density tensor, the angular component of the effective anisotropic density tensor, and the effective bulk modulus, respectively.

Because the sound field satisfies the Laplace equation, the superposition principle is satisfied, and the spectrum can then be expanded. Therefore, only plane waves must be calculated to cover a variety of complex situations. Because of the structural design of the capsule, it is convenient to use the undetermined coefficient method in spherical coordinates to solve for the sound field. The incident wave can be expressed as:

$$\Phi_{\text{inc}} = \sum_{n=0}^{\infty} A_0(2n+1)(\text{i})^n j_n(k_0 r)P_n(\cos\theta), \tag{6}$$

where A_0 is a constant determined by the incident wave, k_0 is the wavenumber of the sound wave in the medium of the external environment, j_n is a spherical Bessel function of the first kind of order n, and P_n is the Legendre function of order n.

Similarly, the scattered wave can also be expanded into a linear combination of spherical waves, which can be expressed as follows:

$$\Phi_{\text{sca}} = \sum_{n=0}^{\infty} A_{n,s}(2n+1)(\text{i})^n h_n^{(1)}(k_0 r)P_n(\cos\theta), \tag{7}$$

where $A_{n,s}$ is the coefficient of the scattered sound wave and h_n is a spherical Bessel function of the third kind of order n.

Therefore, the total sound field's sound pressure in the environmental medium can be expressed as:

$$\begin{aligned}\boldsymbol{\Phi}_{\text{tol}} &= \boldsymbol{\Phi}_{\text{inc}} + \boldsymbol{\Phi}_{\text{sca}} = \sum_{n=0}^{\infty}(2n+1)(\text{i})^n[A_0 j_n(k_0 r) \\ &+ A_{n,s} h_n^{(1)}(k_0 r)]P_n(\cos\theta).\end{aligned} \tag{8}$$

Given that the sound wave must propagate to the interior of the controlled structure, elastic boundary conditions should be selected between the medium and the structure, and also between the middle and interior layers of the structure. Mode conversion occurs at the boundary and thus the medium particle displacement satisfies the Navier equation: [72]

$$\nabla^2 u + \frac{\lambda+\mu}{\mu}\frac{\partial}{\partial t}\nabla(\nabla\cdot u) = \frac{1}{c_s^2}\frac{\partial^2 u}{\partial t^2}, \tag{9}$$

where λ and μ are the Lame coefficients, $c_s = \sqrt{\frac{\mu}{\rho_0}}$, u is the velocity, and ρ_0 is the density of the medium of the external environment.

With regard to the velocity potential in the q-th layer, the longitudinal wave velocity potential can be expressed as:

$$\begin{aligned}\boldsymbol{\Phi}_q &= \sum_{n=0}^{\infty}(2n+1)(\text{i})^n[A_{n,qa} j_n(k_{q1} r) \\ &+ A_{n,qb} n_n(k_{q1} r)]P_n(\cos\theta).\end{aligned} \tag{10}$$

The corresponding transverse wave velocity potential can be expressed as:

$$\begin{aligned}\boldsymbol{\Psi}_q &= \sum_{n=0}^{\infty}(2n+1)(\text{i})^n[A_{n,qc} j_n(k_{q2} r) \\ &+ A_{n,qd} n_n(k_{q2} r)]\frac{dP_n(\cos\theta)}{d\theta},\end{aligned} \tag{11}$$

where $A_{n,qa}$, $A_{n,qb}$, $A_{n,qc}$, and $A_{n,qd}$ are pending parameters, and k_{q1} and k_{q2} are the longitudinal wavenumber and the transverse wavenumber in the q-th spherical shell, respectively.

If the q-th layer is the innermost layer, then the Neumann function item returns to zero, and the velocity potentials in the q-th spherical shell can be written as follows. The longitudinal wave velocity potential can be written as:

$$\boldsymbol{\Phi} = \sum_{n=0}^{\infty}(2n+1)(\text{i})^n A_{n,qa} j_n(k_{q1} r)P_n(\cos\theta). \tag{12}$$

The transverse wave velocity potential can be written as:

$$\boldsymbol{\Psi} = \sum_{n=0}^{\infty}(2n+1)(\text{i})^n A_{n,qc} j_n(k_{q2} r)\frac{dP_n(\cos\theta)}{d\theta}. \tag{13}$$

For the discretized multilayered spherical encapsulant composed of m layers, there are $4(m-1)+3 = 4m-1$ independent boundary condition equations and $4m+1-2 = 4m-1$ undetermined coefficients must also be determined. Therefore, this system of equations is mathematically solvable. The boundary conditions of this structure can then be analyzed in detail. The specific continuity equations and the expansions of the corresponding parameters are given as follows. First, we consider the boundary conditions between the first layer structure and the external medium. The normal velocity continuity can be expressed as:

$$\begin{aligned}u_{r0} &= \frac{\partial\boldsymbol{\Phi}_{\text{tol}}}{\partial r} = \frac{\partial(\boldsymbol{\Phi}_{\text{inc}}+\boldsymbol{\Phi}_{\text{sca}})}{\partial r}, \\ u_{r1} &= \frac{\partial\boldsymbol{\Phi}_1}{\partial r} + \frac{1}{r\sin\theta}\frac{\partial\boldsymbol{\Psi}_1}{\partial\theta}, \\ u_{r0} &= u_{r1}.\end{aligned} \tag{14}$$

The normal stress continuity can be expressed as:

$$\begin{aligned}\sigma_{r0} &= (2\mu+\lambda)\frac{\partial^2\boldsymbol{\Phi}_{\text{tol}}}{\partial r^2} + \lambda\frac{\partial^2\boldsymbol{\Phi}_{\text{tol}}}{\partial r\partial\theta} \\ &= (2\mu+\lambda)\frac{\partial^2(\boldsymbol{\Phi}_{\text{inc}}+\boldsymbol{\Phi}_{\text{sca}})}{\partial r^2} + \lambda\frac{\partial^2(\boldsymbol{\Phi}_{\text{inc}}+\boldsymbol{\Phi}_{\text{sca}})}{\partial r\partial\theta}, \\ \sigma_{r1} &= 2\mu\frac{\partial u_r}{\partial r} + \lambda(\nabla\cdot u) \\ &= (2\mu+\lambda)\left(\frac{\partial^2\boldsymbol{\Phi}_1}{\partial r^2} - \frac{1}{r^2\sin\theta}\frac{\partial\boldsymbol{\Psi}_1}{\partial\theta} + \frac{1}{r\sin\theta}\frac{\partial^2\boldsymbol{\Psi}_1}{\partial\theta\partial r}\right)+ \\ &\lambda\left(\frac{\partial^2\boldsymbol{\Phi}_1}{\partial r\partial\theta} + \frac{-\cos\theta}{r\sin^2\theta}\frac{\partial\boldsymbol{\Psi}_1}{\partial\theta} + \frac{1}{r\sin\theta}\frac{\partial^2\boldsymbol{\Psi}_1}{\partial\theta^2}\right), \\ \sigma_{r0} &= \sigma_{r1}.\end{aligned} \tag{15}$$

Next, we consider the boundary conditions between the q-th layer structure and the q+1-th layer structure. The normal velocity continuity can be expressed in this case as:

$$\begin{aligned} u_{r,q} &= \frac{\partial \boldsymbol{\Phi}_q}{\partial r} + \frac{1}{r\sin\theta}\frac{\partial \boldsymbol{\Psi}_q}{\partial \theta}, \\ u_{r,q+1} &= \frac{\partial \boldsymbol{\Phi}_{q+1}}{\partial r} + \frac{1}{r\sin\theta}\frac{\partial \boldsymbol{\Psi}_{q+1}}{\partial \theta}, \\ u_{r,q}(r_{q,q+1}) &= u_{r,q+1}(r_{q,q+1}), \end{aligned} \tag{16}$$

where $u_{r,q}(r_{q,q+1})$ represents the value of $u_{r,q}$ at the junction between layer q and layer $q+1$. The tangential velocity continuity can be expressed as:

$$\begin{aligned} u_{\theta,q} &= \frac{1}{r}\frac{\partial \boldsymbol{\Phi}_q}{\partial \theta} - \frac{1}{r}\frac{\partial (r\boldsymbol{\Psi}_q)}{\partial r}, \\ u_{\theta,q+1} &= \frac{1}{r}\frac{\partial \boldsymbol{\Phi}_{q+1}}{\partial \theta} - \frac{1}{r}\frac{\partial (r\boldsymbol{\Psi}_{q+1})}{\partial r}, \\ u_{\theta,q}(r_{q,q+1}) &= u_{\theta,q+1}(r_{q,q+1}). \end{aligned} \tag{17}$$

The normal stress continuity can be expressed as:

$$\begin{aligned} \sigma_{r,q} &= 2\mu\frac{\partial u_{r,q}}{\partial r} + \lambda\nabla\cdot u_q \\ &= (2\mu+\lambda)\left(\frac{\partial^2 \boldsymbol{\Phi}_q}{\partial r^2} + \frac{1}{r\sin\theta}\frac{\partial^2 \boldsymbol{\Psi}_q}{\partial r\partial\theta} - \frac{1}{r^2\sin\theta}\frac{\partial \boldsymbol{\Psi}_q}{\partial\theta}\right) \\ &+ \lambda\left(\frac{1}{r}\frac{\partial^2 \boldsymbol{\Phi}_q}{\partial\theta^2} - \frac{1}{r}\frac{\partial \boldsymbol{\Psi}_q}{\partial\theta} - \frac{\partial^2 \boldsymbol{\Psi}_q}{\partial\theta\partial r}\right), \\ \sigma_{r,q+1} &= 2\mu\frac{\partial u_{r,q+1}}{\partial r} + \lambda\nabla\cdot u_{q+1} \\ &= (2\mu+\lambda)\left(\frac{\partial^2 \boldsymbol{\Phi}_{q+1}}{\partial r^2} + \frac{1}{r\sin\theta}\frac{\partial^2 \boldsymbol{\Psi}_{q+1}}{\partial r\partial\theta} - \frac{1}{r^2\sin\theta}\frac{\partial \boldsymbol{\Psi}_{q+1}}{\partial\theta}\right) \\ &+ \lambda\left(\frac{1}{r}\frac{\partial^2 \boldsymbol{\Phi}_{q+1}}{\partial\theta^2} - \frac{1}{r}\frac{\partial \boldsymbol{\Psi}_{q+1}}{\partial\theta} - \frac{\partial^2 \boldsymbol{\Psi}_{q+1}}{\partial\theta\partial r}\right), \\ \sigma_{r,q}(r_{q,q+1}) &= \sigma_{r,q+1}(r_{q,q+1}), \end{aligned} \tag{18}$$

where u_q represents the particle vibration velocity of layer q. The tangential stress continuity can be expressed as:

$$\begin{aligned} \sigma_{\theta,q} &= \mu\left(\frac{1}{r}\frac{\partial u_{r,q}}{\partial\theta} + \frac{\partial u_{\theta,q}}{\partial r} - \frac{u_{\theta,q}}{r}\right) \\ &= \frac{\mu}{r}\left[2\frac{\partial^2 \boldsymbol{\Phi}_q}{\partial r\partial\theta} + \frac{1}{r\sin\theta}\frac{\partial^2 \boldsymbol{\Psi}_q}{\partial\theta^2}\right. \\ &\left. - \frac{\cos\theta}{r\sin\theta^2}\frac{\partial \boldsymbol{\Psi}_q}{\partial\theta} - \frac{2}{r}\frac{\partial \boldsymbol{\Phi}_q}{\partial\theta} + \frac{2}{r}\boldsymbol{\Psi}_q - r\frac{\partial^2 \boldsymbol{\Psi}_q}{\partial r^2}\right], \\ \sigma_{\theta,q+1} &= \mu\left(\frac{1}{r}\frac{\partial u_{r,q+1}}{\partial\theta} + \frac{\partial u_{\theta,q+1}}{\partial r} - \frac{u_{\theta,q+1}}{r}\right) \\ &= \frac{\mu}{r}\left[2\frac{\partial^2 \boldsymbol{\Phi}_{q+1}}{\partial r\partial\theta} + \frac{1}{r\sin\theta}\frac{\partial^2 \boldsymbol{\Psi}_{q+1}}{\partial\theta^2}\right. \\ &\left. - \frac{\cos\theta}{r\sin\theta^2}\frac{\partial \boldsymbol{\Psi}_{q+1}}{\partial\theta} - \frac{2}{r}\frac{\partial \boldsymbol{\Phi}_{q+1}}{\partial\theta} + \frac{2}{r}\boldsymbol{\Psi}_{q+1} - r\frac{\partial^2 \boldsymbol{\Psi}_{q+1}}{\partial r^2}\right], \\ \sigma_{\theta,q}(r_{q,q+1}) &= \sigma_{\theta,q+1}(r_{q,q+1}), \end{aligned} \tag{19}$$

where $u_{r,q}$ is the radial component of the particle vibration velocity in layer q, $u_{\theta,q}$ is the angular component of the particle vibration velocity in layer q, $\boldsymbol{\Phi}_q$ is the longitudinal velocity potential in layer q, and $\boldsymbol{\Psi}_q$ is the transverse velocity potential in layer q.

Therefore, the velocity potential field information that is scattered by the multilayered spherical encapsulant is obtained. Based on this definition, the expression for the ARF on the multilayered spherical encapsulant can be expressed as: [73]

$$\begin{aligned} \mathbf{F} &= \iint_s (p-p_0)\mathbf{n}\mathrm{d}s = \iint_s \rho_0\frac{\partial \boldsymbol{\Phi}_{\mathrm{tol}}}{\partial t}\mathbf{n}\mathrm{d}s \\ &+ \iint_s \frac{1}{2}\rho_0\left(\frac{\partial \boldsymbol{\Phi}_{\mathrm{tol}}}{\partial z}\right)^2\mathbf{n}\mathrm{d}s - \iint_s \frac{1}{2}\frac{\rho_0}{c_0^2}\left(\frac{\partial \boldsymbol{\Phi}_{\mathrm{tol}}}{\partial t}\right)^2\mathbf{n}\mathrm{d}s, \end{aligned} \tag{20}$$

where z is the propagation direction of the incident sound beam, $\mathbf{n}$ is the unit direction vector in the z direction, and c_0 is the sound velocity in the external environment medium.

The algorithm above represents the method used to realize the acoustic capsule structure, which can be verified to be feasible via the subsequent comparison of the theoretical solutions with the numerical calculation results. However, in practical applications, simulation calculations that involve such huge amounts of computation are unacceptable, and thus the ARF can be equivalent to the

Table 1
List of fixed parameters used in the simulations.

Parameter	Symbols	Numerical value
Density of $CaBr_2$	ρ_C	3.15×10^3 kg/m^3
Sound speed of $CaBr_2$	c_C	3140 m/s
Density of $BaSO_4$	ρ_B	4.50×10^3 kg/m^3
Sound speed of $BaSO_4$	c_B	4040 m/s
Density of glycerol	ρ_g	1.26×10^3 kg/m^3
Sound speed of glycerol	c_g	1904 m/s
Density of protein	ρ_p	1.32×10^3 kg/m^3
Sound speed of protein	c_p	1443 m/s
Density of water	ρ_0	1.0×10^3 kg/m^3
Sound speed of water	c_0	1480 m/s

ARF derivation based on the two-layer structure when using the equivalent parameters, i.e., the capsule structure can be regarded as an equivalent uniform parameter layer. This rationality is also verified in the subsequent finite element simulations. The mechanical parameters of the equivalent structure can be adjusted by varying each parameter in the equivalent formula, which allows precise control of the ARF to be achieved via selection of the mechanical parameters for each layer of the structure.

3. Theoretical solution and finite element simulation

In both the finite element simulation and the theoretical solution in this section, the background material is considered to be water. The inner radius of the acoustic capsule is 1 mm and its outer radius is 2 mm. The thickness ratio here is 1 : 1. In subsections A and B, the incident frequency is fixed at 2 MHz. The material parameters are given in Table 1 and these parameters will be used below unless otherwise specified.

Two payloads with different acoustic parameters can both obtain the same ARF during transport, which illustrates the feasibility of the proposed acoustic capsule design well. Therefore, in subsections A and B, $BaSO_4$ and $CaBr_2$ are initially selected as the payloads. As a result of its good radioactive absorption capacity, $BaSO_4$ is often used as a vascular and gastrointestinal contrast agent. $CaBr_2$ is a sedative drug that is used commonly in the treatment of cardiovascular and cerebrovascular diseases, e.g., epilepsy. To provide further verification of the possibility of transport of drugs with parameters that are close to those of the environmental medium, two organic drug materials (glycerol and protein) are selected as the payloads in subsection B.

3.1. Verification of the rationality of equivalent anisotropy and the existence of the acoustic capsule using a multilayered encapsulant

Here, the acoustic capsule is constructed. The payload in this case is $BaSO_4$. Using the finite element simulation software COMSOL 6.1, the model shown in Fig. 1 is set up. The mesh size for the finite element simulation is limited by the wavelength and the maximum grid size here does not exceed one-sixth of the wavelength. The maximum cell growth rate in this case is 1.5. The curvature factor is 0.6. The narrow area resolution is 0.5. During boundary handling, iterations for a smooth transition are added to the internal meshes. The number of iterations here is four. The division method for the surface mesh is quadrilateral and the number of iterations used in the sweeping process during modeling is four. Sharp edges are handled by splitting. The minimum angle that is split during the splitting process is 240 degrees and the maximum angle obtained via splitting is 100 degrees. The ideal equivalent parameters for the capsule material are the directly given anisotropic equivalent parameters. Both the 50-layer and 20-layer capsule materials use homogeneous materials to simulate the anisotropic materials based on Eqs. (4) and (5). The thickness of each layer is the same. The acoustic scattering field can be determined based on the model and the ARF is calculated using the acoustic scattering field. As selected based on Eqs. (4) and (5), the two material parameters that constitute the acoustic capsule in the simulations are given by the following equations:

$$\begin{aligned}
\rho_A &= \rho_r \frac{r + \sqrt{2ra - a^2}}{r - a} \\
\rho_B &= \frac{\rho_r^2}{\rho_A} \\
c_A = c_B &= c_r \frac{(b-a)}{b} \frac{r}{r-a} \\
\kappa_A &= \rho_A c_A^2 \\
\kappa_B &= \rho_B c_B^2 \\
\kappa &= \frac{2\kappa_A \kappa_B}{\kappa_A + \kappa_B},
\end{aligned} \tag{21}$$

where ρ_r and c_r are the equivalent parameters of the acoustic capsule and are given with the different simulation cases.

In Fig. 2, the results of finite element simulations with different equivalent parameters are illustrated. In the examples shown in Fig. 2 with subscripts 1, 2 and 3, $BaSO_4$ particles are encapsulated by the acoustic capsules. The densities and sound velocities of the starch capsule shells and gelatin capsule shells that are commonly used in medicine are greater than those of the environmental

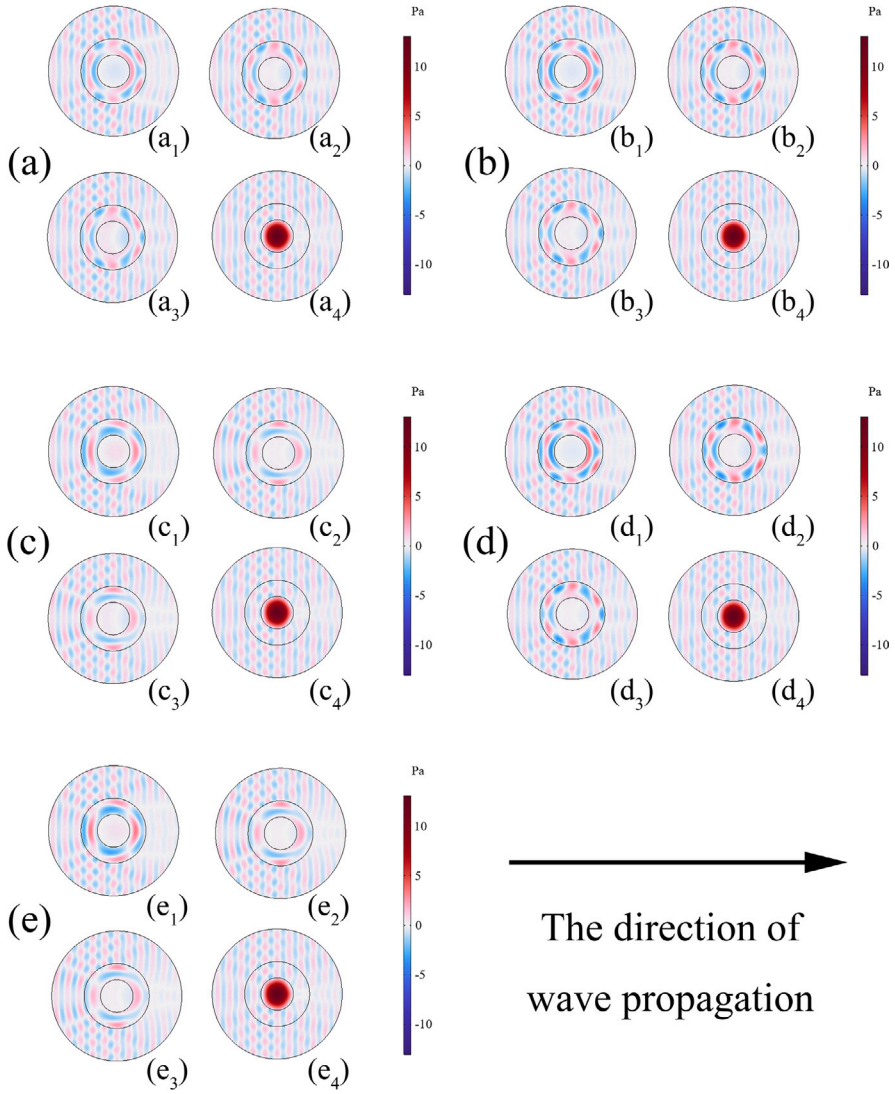

Fig. 2. Sound field distributions of acoustic capsules carrying a $BaSO_4$ particle with different equivalent density and sound velocity values given, respectively, by: (a) 2000 kg/m^3 and 2500 m/s; (b) 2500 kg/m^3 and 2500 m/s; (c) 2500 kg/m^3 and 3000 m/s; (d) 3000 kg/m^3 and 2500 m/s; and (e) 3000 kg/m^3 and 3000 m/s, respectively. The sound fields are shown in: (a_1), $(b_1)\ldots(e_1)$ for an acoustic capsule with uniform heterogeneous parameters; (a_2), $(b_2)\ldots(e_2)$ for an acoustic capsule with a 50-layer structure imitation; and (a_3), $(b_3)\ldots(e_3)$ for an acoustic capsule with an 20-layer structure imitation. In addition, (a_4), $(b_4)\ldots(e_4)$ serve as the control group here, where the particles are exposed to the sound field directly without the acoustic capsule.

materials. Therefore, we selected material parameters with density and sound velocity values that are greater than those of water to verify the feasibility of the acoustic capsule design. To provide a more convincing example and cause the scattering phenomenon to be more obvious to produce larger ARFs, parameters that were very close to the parameters of the environment medium were not selected in this case. At the same time, to provide a better illustration of the superiority of the proposed scheme, a large parameter span was also selected. Five combinations of parameters were used, for acoustic capsules with: equivalent density of 2000 kg/m^3 and equivalent sound velocity of 2500 m/s; equivalent density of 2500 kg/m^3 and values of the equivalent sound velocity of 2500 m/s and 3000 m/s; equivalent density of 3000 kg/m^3 and values of the equivalent sound velocity of 2500 m/s and 3000 m/s. The resulting fields are shown in Fig. 2 as follows: The subfigures with subscript 1, 2 and 3, represent the acoustic capsule with, respectively: (1) uniform heterogeneous parameters, (2) the 50-layer structure imitation and (3) the 20-layer structure imitation. In the subfigures with subscript 4, the $BaSO_4$ particles are exposed to the sound field directly without the acoustic capsule, i.e., the areas occupied by the acoustic capsules in the other subfigures are replaced by the surrounding medium. Moreover, the capsule design scheme proposed in this paper is also feasible when other equivalent parameter ranges are used. The results obtained for each equivalent parameter show that it is reasonable to use a layered structure to realize the anisotropic equivalent parameters of the acoustic capsules; in particular, the sound field obtained when using the 50-layer structure is almost identical to that obtained with the perfect equivalent parameters. The simulation of the 20-layer structure was performed because we wanted to show that when the control accuracy

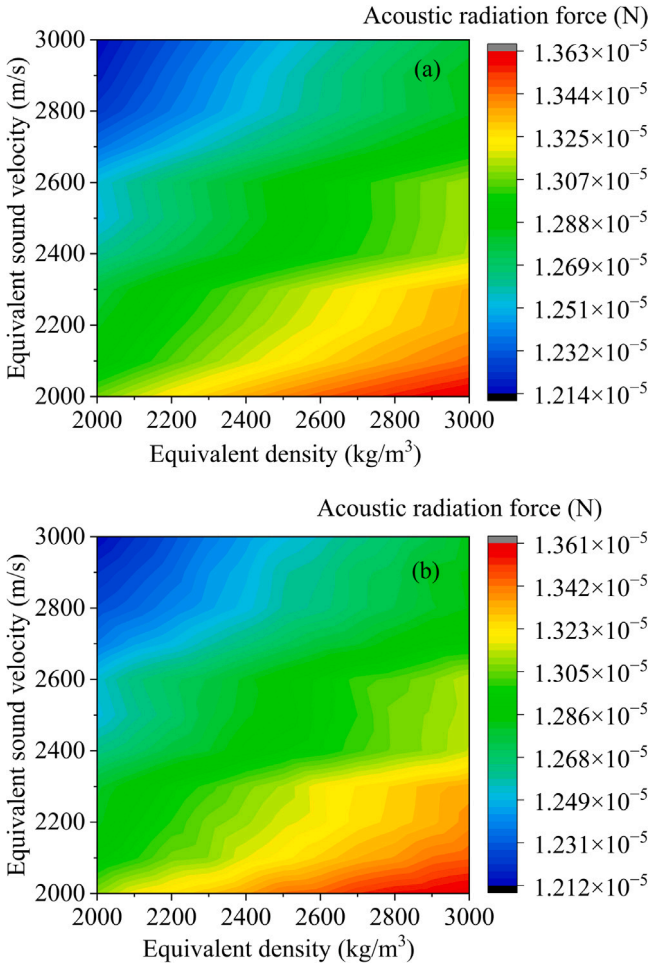

Fig. 3. Comparison of ARF characteristics obtained by (a) an ideal anisotropic acoustic capsule structure and (b) a 50-layer acoustic capsule structure with different equivalent parameters when carrying a $BaSO_4$ particle.

requirements are not very strict, a satisfactory effect can still be achieved by reducing the number of layers appropriately to reduce both the process difficulty and the process cost.

In Fig. 2, we used five sets of different equivalent parameters to perform the finite element simulations. For each set of equivalent parameters, we conducted comparisons that involved three scenarios: an equivalent single-layer structure, a 20-layer structure, and a 50-layer structure. From the acoustic field distributions, it was clearly visible that these three scenarios all exhibited identical field patterns within the permissible error range. Consequently, we assert here that the finite element simulation results support the effectiveness of the application of equivalent parameter methods to acoustic field analysis of multilayered spherical shell structures and their responses to acoustic excitations.

To verify the ARF value obtained by the capsule, according to the theory given in Section 2, theoretical calculations for the 50-layer acoustic capsule structure and the ideal anisotropic acoustic capsule structure were performed, and the results obtained are shown in Fig. 3.

The image in Fig. 3(a) represents the ARF obtained by an ideal anisotropic acoustic capsule structure and that in Fig. 3(b) represents the ARF obtained by an acoustic capsule modeled on the 50-layer structure. Comparison shows that the two results are basically consistent, which thus verifies that it is both reasonable and feasible to use a layered structure to realize a anisotropic acoustic capsule.

3.2. Acoustic capsules carrying different transported particles

The intention of the acoustic capsule design is to enable the capsule to carry any object and cause any object to obtain the same ARF. Therefore, a finite element simulation of the sound field distribution of the acoustic capsule when carrying a $CaBr_2$ particle was conducted, with results as shown in Fig. 4.

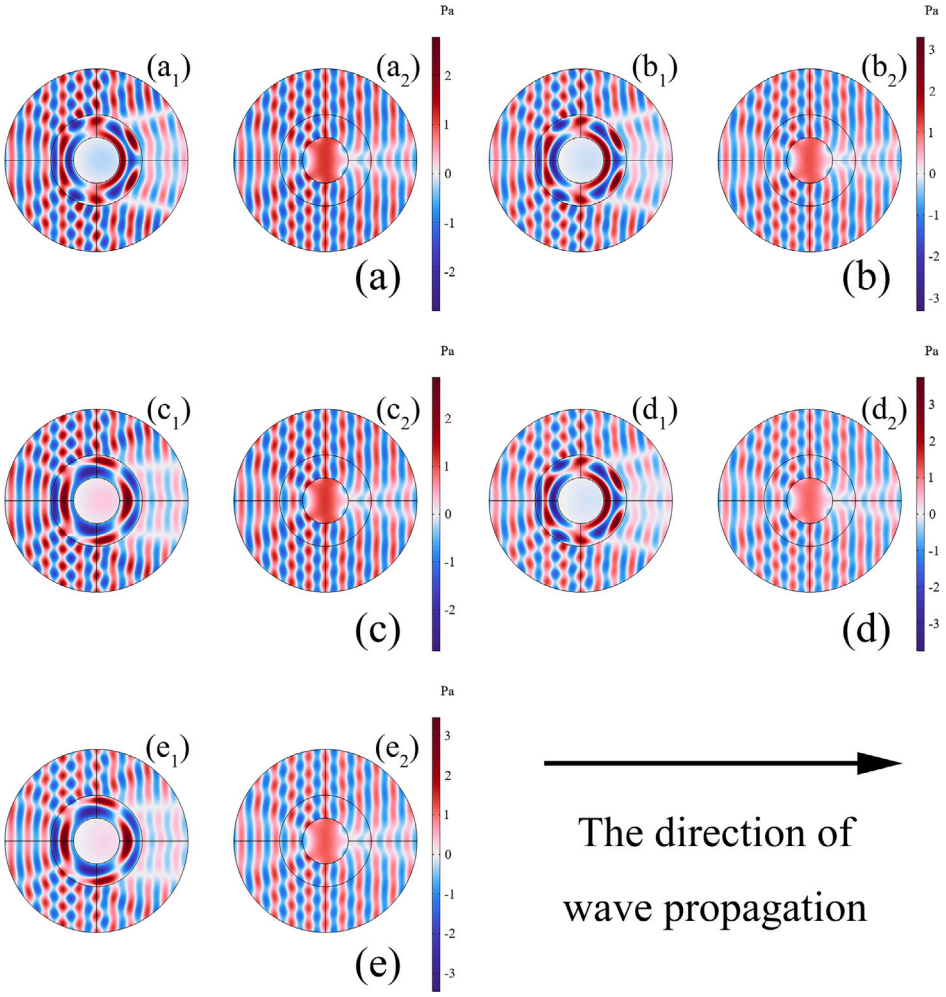

Fig. 4. Sound field distributions of acoustic capsules carrying a $CaBr_2$ particle with different equivalent density and sound velocity values given, respectively, by (a_1) 2000 kg/m^3 and 2500 m/s; (b_1) 2500 kg/m^3 and 2500 m/s; (c_1) 2500 kg/m^3 and 3000 m/s; (d_1) 3000 kg/m^3 and 2500 m/s; and (e_1) 3000 kg/m^3 and 3000 m/s. (a_2), (b_2)...(e_2) serve as the control group here, where particles are exposed to the sound field directly without the acoustic capsule.

In Fig. 4, similar to the results in Fig. 2, the sound pressure distributions of the acoustic capsules with different equivalent parameters when carrying a $CaBr_2$ particle in the sound field are shown. In the examples where the particle is exposed to the sound field directly, the area in which the acoustic capsule was present is replaced by the surrounding medium. The sound field distributions of the $CaBr_2$ particle when carried by the acoustic capsule structure are shown in Fig. 4(a_1), (b_1)...(e_1), while the corresponding cases in which the $CaBr_2$ particle is exposed to the sound field directly without the acoustic capsule structure are shown in Fig. 4(a_2), (b_2)...(e_2). Comparison of Fig. 2 with Fig. 4 shows that the external sound field structures of the acoustic capsules with the same equivalent parameters are essentially the same. For the cases where the $BaSO_4$ and $CaBr_2$ particles were exposed to the sound field directly, the ARFs obtained would differ significantly.

To provide further verification of the feasibility of medical application of this technique, in a manner similar to that shown in Fig. 4, the sound field distributions of acoustic capsules with different equivalent parameters when carrying a glycerol particle and a protein particle are plotted in Fig. 5 and Fig. 6, respectively.

Similar to Fig. 2, in the examples where the particles are exposed to the sound field of the medium directly, the area occupied by the acoustic capsule is again replaced by the surrounding medium. Comparison of Fig. 2 with Fig. 4, Fig. 5, and Fig. 6 shows that the external sound field structures of the acoustic capsule structures with the same equivalent parameters are basically the same. For particles composed of different materials that are exposed to the sound field directly, the ARFs obtained will differ significantly.

Furthermore, based on the theory given in Section 2, the ARF obtained when the anisotropic acoustic capsule structure was used to transport a $CaBr_2$ particle was calculated, with results as shown in Fig. 7(a). To demonstrate the feasibility of practical applications of this technique in medicine, glycerol and protein were also selected as payloads, and the corresponding characteristics were obtained as shown in Fig. 7(b) and Fig. 7(c), respectively.

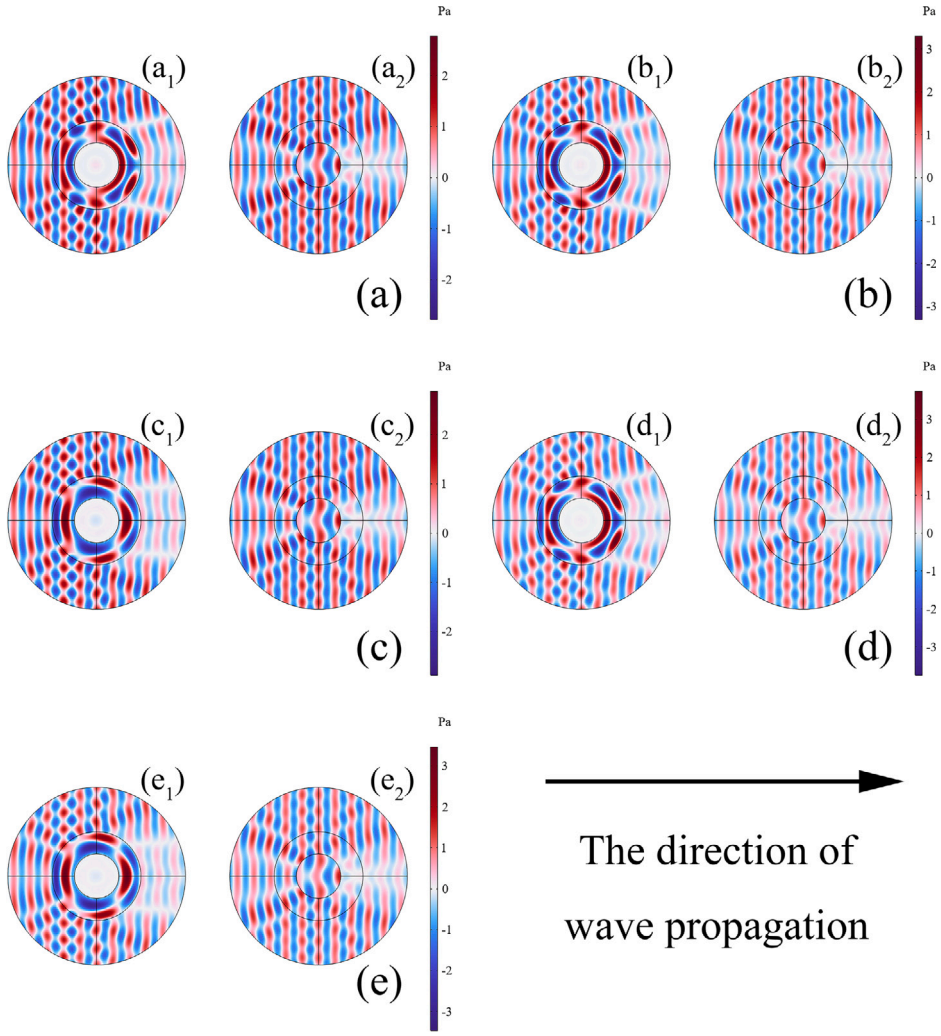

Fig. 5. Sound field distributions of acoustic capsules when carrying a glycerol particle with different equivalent densities and sound velocities given, respectively, by (a_1) 2000 kg/m^3 and 2500 m/s; (b_1) 2500 kg/m^3 and 2500 m/s; (c_1) 2500 kg/m^3 and 3000 m/s; (d_1) 3000 kg/m^3 and 2500 m/s; and (e_1) 3000 kg/m^3 and 3000 m/s. (a_2), (b_2)…(e_2) serve as the control group here, where the particles are exposed to the sound field directly without the acoustic capsule.

In Fig. 7, the ARF characteristics obtained for the acoustic capsule with different equivalent densities and equivalent sound velocities when transporting different particles are plotted. It can be seen from Figs. 3 and 7 that the ARFs obtained when carrying the different particles are basically the same. This verifies that the acoustic capsule concept is feasible; the acoustic capsule can carry the objects to be transported with different acoustic parameters and the ARF obtained by the capsule structure when carrying these transported objects is only related to the equivalent parameters of the capsule itself. Regardless of the differences between the parameters of the payloads, the ARF acting on the acoustic capsule and on the payload as a whole remains constant.

Comparison of Figs. 3 and 7 clearly shows that acoustic capsules with specifically designed anisotropic parameters could appear to have the same sound field response while loaded with different objects, which also verifies the correctness of our theoretical design.

3.3. Law of acoustic radiation force variation with frequency spectrum

The design parameters that can be adjusted include not only the equivalent density and the equivalent sound velocity of the acoustic capsule structure itself, but also the maximum ARF, which can be varied by adjusting the frequency spectrum of the incident sound wave. According to the theory presented in Section 2, we calculated the ARFs for the two different capsules under different incident frequency conditions. The equivalent density of the first acoustic capsule was 2500 kg/m^3 and the equivalent sound

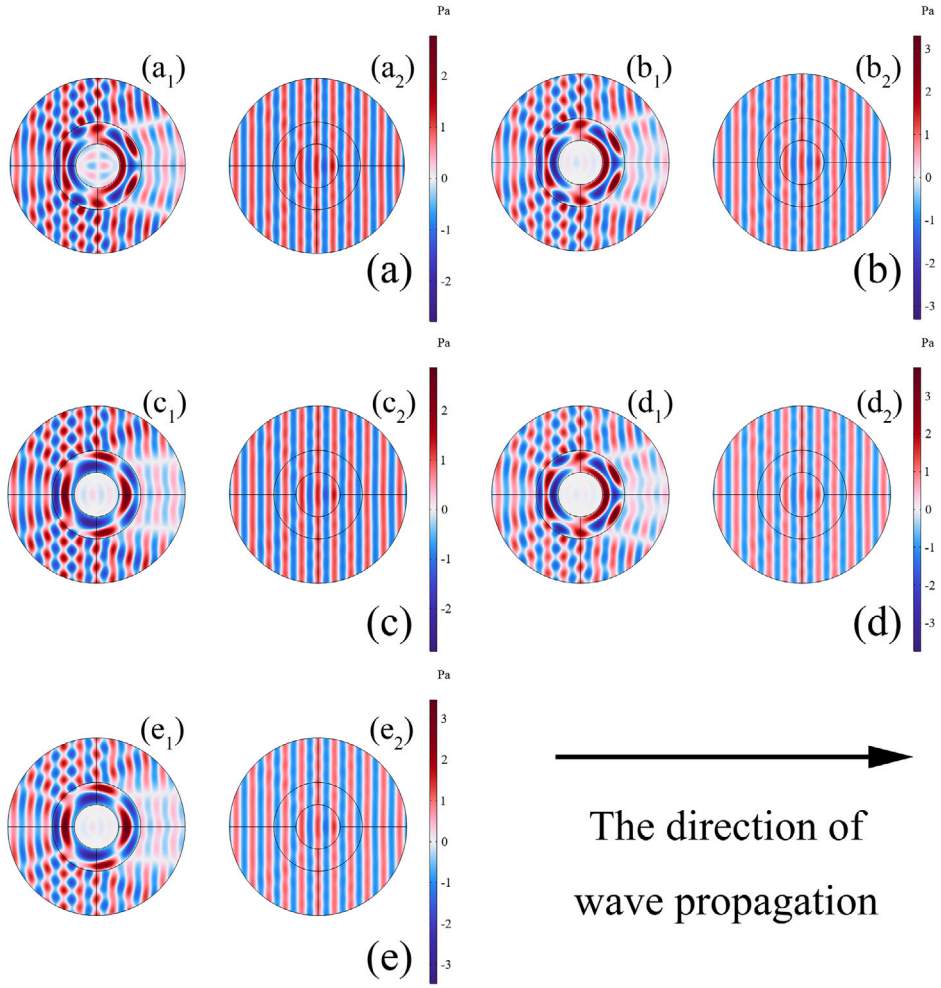

Fig. 6. Sound field distributions of acoustic capsules when carrying a protein particle with different equivalent densities and sound velocities given, respectively, by (a_1) 2000 kg/m^3 and 2500 m/s; (b_1) 2500 kg/m^3 and 2500 m/s; (c_1) 2500 kg/m^3 and 3000 m/s; (d_1) 3000 kg/m^3 and 2500 m/s; and (e_1) 3000 kg/m^3 and 3000 m/s. (a_2), (b_2)...(e_2) serve as the control group here, where particles are exposed to the sound field directly without the acoustic capsule.

velocity was 2500 m/s. The equivalent density of the second acoustic capsule was 3000 kg/m^3 and the equivalent sound velocity was 3000 m/s. The ARFs obtained as a function of the incident frequency are shown in Fig. 8. From Fig. 8, the specific equivalent parameters when the maximum ARF is obtained can be found based on the specific spectrum, which then allows us to obtain the optimal ARF driving effect.

The finite element simulation results shown in Fig. 8 were obtained using a 50-layer spherical shell structure, and these results also verify the consistency of the theory proposed in Section 2 with the finite element simulation results obtained using the COMSOL software. The results obtained by using the equivalent parameter method in the theoretical calculations and via COMSOL using the multilayer structures for the simulations are consistent. This provides a further demonstration of the correctness of the proposed scheme.

In this section, we used two modeling methods in simulation verification. The first was used to assign equivalent anisotropic parameters to the structure directly, as shown in the cases in the upper left corner of each subfigure in Fig. 2 and Fig. 3(a). The second was used to form equivalent anisotropy through use of multilayer (20 or 50 layers) isotropic materials, as shown in the two cases below each subfigure in Fig. 2 and Fig. 3(b). Comparison of the sound fields formed via these two modeling methods shows that the sound field distribution remains basically the same. Therefore, we can confirm that the idea that we proposed is correct: equivalent anisotropy can be realized by arranging multiple layers of isotropic materials periodically according to an equivalent parameters design. By comparing cases where the equivalent parameters are the same but the capsules are carrying different contents, as shown in Fig. 2, Fig. 4, Fig. 5, and Fig. 6, we can see that the sound field distribution again remains basically the same. This verifies that another of our assumptions is correct: i.e., the abnormal phenomenon of carrying different contents but obtaining the same ARF can also be realized through equivalent anisotropy.

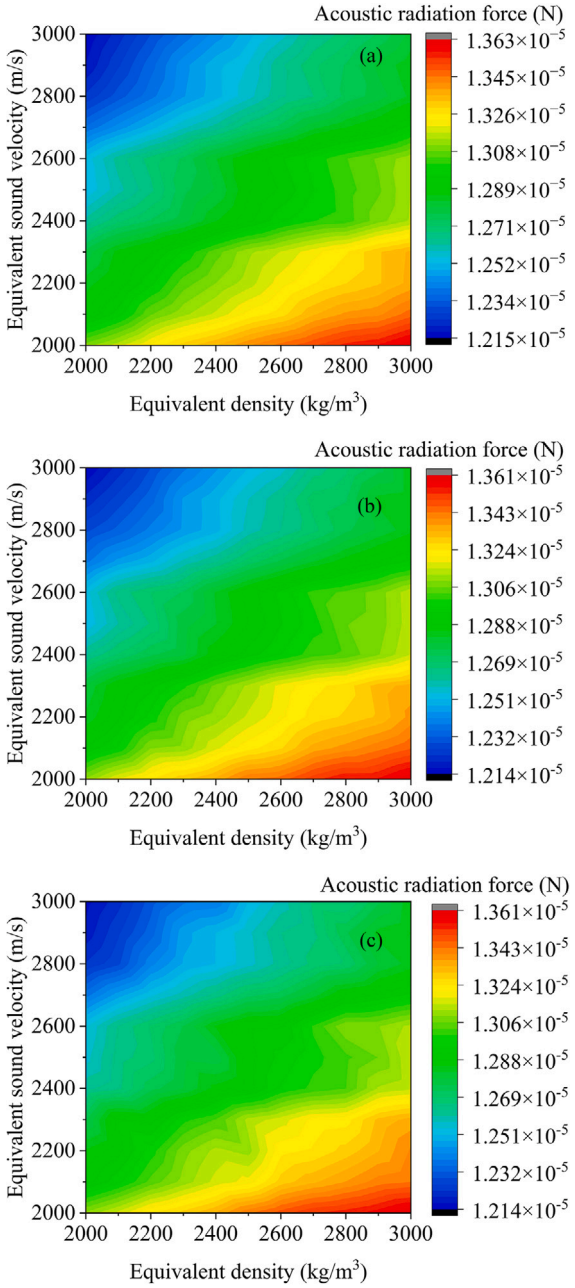

Fig. 7. ARF characteristics obtained by an ideal anisotropic acoustic capsule structure with different equivalent parameters when carrying (a) a $CaBr_2$ particle, (b) a glycerol particle, and (c) a protein particle.

4. Discussion

As verified in Section 3, when the capsule structure has been determined, the ARF received by the capsule and its contents as a whole will be fixed and will remain unaffected by any changes in the contents. The sound field distributions obtained for the same capsule when carrying different particles remain consistent because the sound field does not penetrate the inner cavity of the capsule. Consequently, these internal particles do not influence the magnitude of the ARF.

The selection of the materials for construction of the acoustic capsule is subject to minimal constraints, thus broadening the range of suitable materials for practical applications significantly. By considering factors such as cost and biological adaptability, the layered materials that constitute the acoustic capsule structure can be selected most appropriately. Additionally, when the mass of the internal particles to be transported is fixed, different particles can achieve the same ARF and the same acceleration while

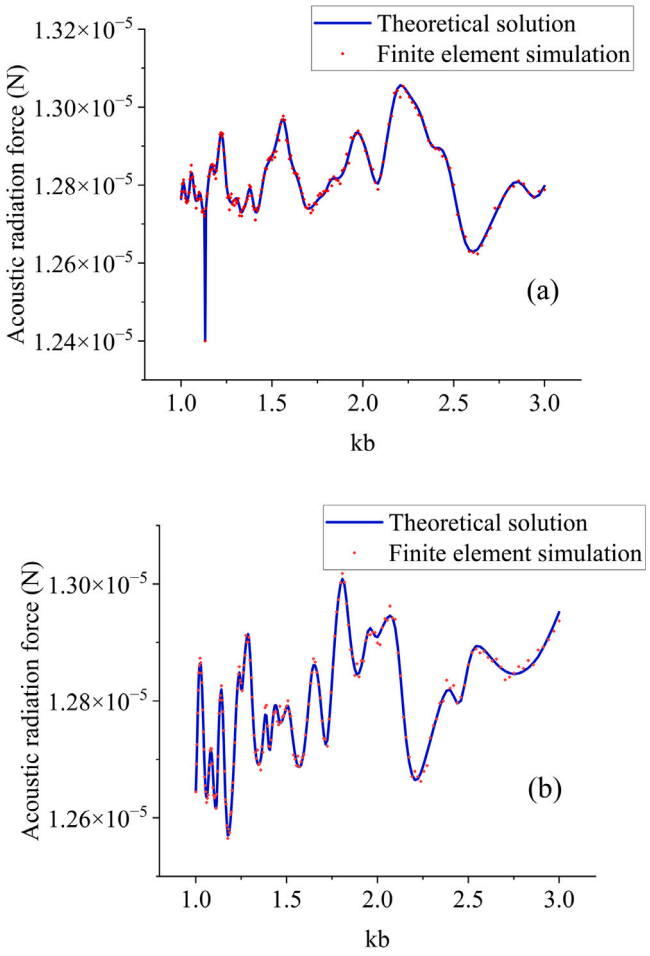

Fig. 8. Variations in ARF obtained by the acoustic capsule with different equivalent densities and equivalent sound velocities, respectively, of (a) 2500 kg/m^3 and 2500 m/s, and (b) 3000 kg/m^3 and 3000 m/s, versus the incident acoustic frequency obtained by theoretical solutions and finite element simulations.

using the same capsule. This would allow for simultaneous transport of different drugs to the same location at the same acceleration, assuming that the interactions between the drug particles can be neglected, and thus potentially could improve treatment efficacy.

In previous studies on negative ARF, there were strict limitations on the diameter of the particles subjected to negative ARF, as well as on the density and sound speed of the particle material [73–78]. These restrictions made it difficult to apply negative ARF in practice. However, the design of the acoustic capsule avoids acoustic interaction between the inside and outside of the capsule, allowing the capsule and its contents as a whole to experience ARF, which depends only on the effective density and effective sound speed of the capsule. Since the acoustic capsule can be designed to meet the specific density and sound speed requirements for achieving negative ARF, it can carry particles with arbitrary parameters (i.e., diameter, density and sound speed) to experience negative ARF, thus enhancing the potential of the negative ARF for practical applications significantly.

In actual industrial production, precision processing of spherical shells into an equal-thickness stack is relatively challenging and may lead indirectly to high economic costs. This is a significant factor that could limit more widespread application of acoustic capsules. In this work, we also simplified the 50-layer scheme down to a 20-layer scheme for the simulations and again obtained good results, thus demonstrating a potential method to reduce costs by reducing the precision appropriately. Although the current cost of processing the capsule design may be high, advancements in technologies including 3D printing and mass production are expected to reduce these costs significantly in the future.

The concept of the "acoustic capsule" is proposed in this work to provide a visual illustration of a structure that is designed to carry any object, much like a conventional capsule. Capsules that are loaded with different objects can achieve the abnormal phenomenon of experiencing the same ARF within the same sound field; we refer to this phenomenon as "uniform transport". Based on consideration of the functional similarity of this structure to a capsule, the term "acoustic capsule" is used here. In medicine, a capsule typically isolates and prevents interactions between substances located inside and outside the capsule. Similarly, an acoustic capsule isolates and prevents acoustic interactions between the substances located inside and outside the capsule. The basic construction method for the acoustic capsule involves use of a multilayer spherical shell structure, which forms an

anisotropic material through the equivalent parameter method. This anisotropic material then enables uniform transport. Based on our theoretical analysis, each layer of the multilayer spherical shell structure participates in the acoustic process. Because the acoustic capsule has the unusual property of providing internal acoustic shielding, the object being carried does not participate in the acoustic process. This is why the same acoustic capsule can experience the same ARF, regardless of the internal structure that it carries. The ARF discussed in this work refers to the force experienced by the capsule as a whole, including the object carried inside the capsule.

Acoustic manipulation based on radiation forces is combined with commonly used equivalent parameter methods in acoustic metamaterials [65–71], thereby enabling the proposal of a capsule structure that is capable of obtaining the same ARF when hosting arbitrary objects. These anomalous characteristics are not typically present in general multilayered spherical shells. Specific constraints and design methods are presented for the capsule design here and the feasibility of the proposed solution is validated through numerical calculations and finite element simulations.

Multiple materials can be used to construct the acoustic capsule to achieve uniform transport of the ARFs. This effect can be achieved as long as the periodic combination of these multiple materials can meet the equivalent parameter requirements. The equivalent parameter calculation formulas for the multiple materials in this case are given by Eqs. (1) and (2). The two-material scheme presented here represents the simplest case and has been proven to be a quite effective scheme in this work. It can also be determined from Eqs. (1) and (2) that the introduction of multiple materials can provide a higher degree of freedom in the design, which lays the foundation for further application of these acoustic capsules in a variety of fields.

As shown in the theoretical section of the work, our material parameter selection process has a high degree of freedom. The number of equations for equivalent parameter expressions that the structure must satisfy is fixed, and thus increasing the types of participating materials can also effectively increase the number of degrees of freedom in the material selection process. The material parameters involved in the optimization scheme are the density, the Young's modulus, and the Poisson's ratio of the material. No physical requirements are placed on the other parameters of the constituent materials. In addition, it can also be seen from Eqs. (3) and (4) that the thickness ratio of the different materials is another adjustable parameter. Because we only need to pay attention to the establishment of the equivalent parameter equations for a variety of material compositions, this represents an indefinite system of equations with a number of undetermined parameters that is far greater than the number of constraints. The optimization results are related to the equivalent parameters and are independent of the actual materials.

Equivalent parameter methods, which are validated and widely used techniques, offer specific constraint equations [65–71]. Upon verification of the applicability of these methods to the designed acoustic capsule, which is composed of multilayered spherical shell structures, the treatment of these structures then simplifies to handling of an isotropic material spherical shell after equivalence. In the theoretical analysis, we have addressed the fact that when equivalent parameter methods applied, parameters such as the layer thicknesses, density ratios, and compression ratios that constitute the multi-layered spherical shell structure affect the final equivalent parameters. Analytical results that support this influence have been provided. Post-application of equivalent parameter methods shows that these parameters (the layer thickness, density ratios, and compression ratios) that form the multilayered spherical shell structure no longer act as independent parameters in influencing the overall structure's feedback to the acoustic field.

In addition to use in liquid and fluid environments, the design of these acoustic capsules can also be used in air. As long as the equivalent parameters satisfy the requirements for the inner shielding effect, acoustic uniform transport can be realized.

The design for the current work was conducted in the medium of and ideal fluid, and thus the theory with regard to thermal thermoviscous losses, attenuation, viscoelasticity, and streaming effects has not been considered to date. The viscosity in the fluid will affect both the outermost boundary conditions and the specific expression for the ARF, but it will not affect establishment of the equivalent parameter relationship. Therefore, when the dissipation caused by the viscosity of the fluid medium is considered, the acoustic capsule will still have the ability to carry different objects and obtain the same ARF. The work described in this manuscript focuses more closely on the design of the internal shielding structure for the acoustic waves, thus providing a feasible idea for standardization of acoustic manipulation processes.

5. Conclusion

In this paper, an acoustic capsule is designed based on the equivalent anisotropy of density and of sound speed. Inner shielding from the sound field is realized by the designed acoustic capsule, which means that any object on board is subjected to the same ARF. A theoretical design method is proposed and is verified using finite element simulations. An idea for design optimization to increase the ARF further and enable selection of suitable materials is proposed, i.e., a specific optimization can be realized through appropriate design of the frequency spectrum of the incident wave and the equivalent mechanical parameters of the acoustic capsule. The proposed design has opened up a new field that enables precise manipulation of different particles based on the ARF. This design has broad application prospects in the fields of life sciences and medicine.

CRediT authorship contribution statement

Menyang Gong: Writing – review & editing, Writing – original draft, Visualization, Validation, Supervision, Software, Resources, Project administration, Methodology, Investigation, Formal analysis, Data curation, Conceptualization. **Yuanyuan Li:** Data curation. **Yupei Qiao:** Data curation. **Xin Xu:** Data curation. **Zhonghan Fei:** Data curation. **Shenlian Gao:** Data curation. **Jiehui Liu:** Methodology. **Aijun He:** Methodology. **Xiaozhou Liu:** Writing – review & editing, Supervision, Resources, Project administration, Funding acquisition.

Declaration of competing interest

No conflict of interest exists in the submission of this manuscript, and the manuscript is approved by all authors for publication. I would like to declare on behalf of my co-authors that the work described in this paper was original research that has not been published previously, and not under consideration for publication elsewhere, in whole or in part. All the authors listed have approved the manuscript that is enclosed.

Data availability

Data will be made available on request.

Acknowledgments

Funding

This work was supported by the National Key R&D program of China [No. 2020YFA0211400]; the State Key Program of National Natural Science of China [No. 11834008]; the National Natural Science Foundation of China [No. 12174192 and No. 12204119]; the State Key Laboratory of Acoustics, Chinese Academy of Sciences [No. SKLA202410]; the Key Laboratory of Underwater Acoustic Environment, Chinese Academy of Sciences [No. SSHJ-KFKT-1701]; and the Guizhou Provincial Science and Technology Foundation [No. ZK[2023]249]. We thank David MacDonald, MSc, from Liwen Bianji (Edanz) (www.liwenbianji.cn) for editing the English text of a draft of this manuscript.

References

[1] P.L. Marston, D.B. Thiessen, Manipulation of fluid objects with acoustic radiation pressure, Ann. New York Acad. Sci. 1027 (2004) 414–434, http://dx.doi.org/10.1196/annals.1324.034.
[2] N. Nama, R. Barnkob, Z.M. Mao, C.J. Kahler, F. Costanzo, T.J. Huang, Numerical study of acoustophoretic motion of particles in a pdms microchannel driven by surface acoustic waves, Lab Chip 15 (12) (2015) 2700–2709, http://dx.doi.org/10.1039/c5lc00231a.
[3] A. Pavlic, P. Nagpure, L. Ermanni, J. Dual, Influence of particle shape and material on the acoustic radiation force and microstreaming in a standing wave, Phys. Rev. E 106 (1) (2022) 015105, http://dx.doi.org/10.1103/PhysRevE.106.015105.
[4] C. Goering, J. Dual, Measuring the effects of a pulsed excitation on the buildup of acoustic streaming and the acoustic radiation force utilizing an optical tweezer, Phys. Rev. E 105 (5) (2022) 055103, http://dx.doi.org/10.1103/PhysRevE.105.055103.
[5] H. Tanaka, K. Funayama, Y. Tadokoro, Periodic switching of acoustic radiation force with beat created by multitone field, Sci. Rep. 12 (1) (2022) 15029, http://dx.doi.org/10.1038/s41598-022-19077-9.
[6] A. Alhyari, C. Gorg, C.F. Dietrich, C. Trenker, M. Ludwig, E.S. Zadeh, Diagnostic performance of point shear wave elastography using acoustic radiation force impulse technology in peripheral pulmonary consolidations: A feasibility study, Ultrasound Med. Biol. 48 (5) (2022) 778–785, http://dx.doi.org/10.1016/j.ultrasmedbio.2021.12.015.
[7] S.G. Zhao, M.X. Wu, S.J. Yang, Y.Q. Wu, Y.Y. Gu, C.Y. Chen, J. Ye, Z.M. Xie, Z.H. Tian, H. Bachman, P.H. Huang, J.P. Xia, P.R. Zhang, H.Y. Zhang, T.J. Huang, A disposable acoustofluidic chip for nano/microparticle separation using unidirectional acoustic transducers, Lab Chip 20 (7) (2020) 1298–1308, http://dx.doi.org/10.1039/d0lc00106f.
[8] M. Azarpeyvand, M. Azarpeyvand, Acoustic radiation force on a rigid cylinder in a focused Gaussian beam, J. Sound Vib. 332 (9) (2013) 2338–2349, http://dx.doi.org/10.1016/j.jsv.2012.11.002.
[9] T.Q. Tang, L.X. Huang, Acoustic radiation force for multiple particles over a wide size-scale by multiple ultrasound sources, J. Sound Vib. 509 (2021) 116256, http://dx.doi.org/10.1016/j.jsv.2021.116256.
[10] T.Q. Tang, L.X. Huang, An efficient semi-analytical procedure to calculate acoustic radiation force and torque for axisymmetric irregular bodies, J. Sound Vib. 532 (2022) 117012, http://dx.doi.org/10.1016/j.jsv.2022.117012.
[11] Y.G. Qu, J.P. Su, H.X. Hua, G. Meng, Structural vibration and acoustic radiation of coupled propeller-shafting and submarine hull system due to propeller forces, J. Sound Vib. 401 (2017) 76–93, http://dx.doi.org/10.1016/j.jsv.2017.03.034.
[12] H.B. Wang, Y.P. Qiao, J.H. Liu, B. Jiang, G.T. Zhang, C.W. Zhang, X.H. Liu, Experimental study of the difference in deformation between normal and pathological, renal and bladder, cells induced by acoustic radiation force, Eur. Biophys. J. Biophy. 49 (2) (2020) 155–161, http://dx.doi.org/10.1007/s00249-020-01422-3.
[13] M.W. Urban, Production of acoustic radiation force using ultrasound: methods and applications, Expert Rev. Med. Devices 15 (11) (2018) 819–834, http://dx.doi.org/10.1080/17434440.2018.1538782.
[14] M.L. Palmeri, K.R. Nightingale, Acoustic radiation force-based elasticity imaging methods, Interface Focus 1 (4) (2011) 553–564, http://dx.doi.org/10.1098/rsfs.2011.0023.
[15] M. Tozaki, S. Isobe, E. Fukuma, Preliminary study of ultrasonographic tissue quantification of the breast using the acoustic radiation force impulse (ARFI) technology, Eur. J. Radiol. 80 (2) (2011) E182–E187, http://dx.doi.org/10.1016/j.ejrad.2011.05.020.
[16] J.Y. Gu, L.F. Du, M. Bai, H.L. Chen, X. Jia, J. Zhao, X.M. Zhang, Preliminary study on the diagnostic value of acoustic radiation force impulse technology for differentiating between benign and malignant thyroid nodules, J. Ultrasound Med. 31 (5) (2012) 763–771.
[17] F. Eslami, H. Hamzehpour, S. Derikvandi, S.A. Bahrani, Acoustic interaction force between two particles immersed in a viscoelastic fluid, Phys. Fluids 35 (3) (2023) 031707, http://dx.doi.org/10.1063/5.0143005.
[18] G. Regnault, A.A. Doinikov, C. Mauger, P. Blanc-Benon, C. Inserra, Dynamics of two interacting acoustic bubbles at short separation distances, Phys. Fluids 35 (3) (2023) 037116, http://dx.doi.org/10.1063/5.0135370.
[19] Y.C. Kim, P. Blanloeuil, D.D. Li, R.A. Taylor, T.J. Barber, Acoustically driven translation of a single bubble in pulsed traveling ultrasonic waves, Phys. Fluids 35 (3) (2023) 033315, http://dx.doi.org/10.1063/5.0138484.
[20] L. Rayleigh, On the momentum and pressure of gaseous vibrations, and on the connecion with the virial theorem., Phil. Mag. 10 (55–60) (1905) 364–374, http://dx.doi.org/10.1080/14786440509463381.
[21] L.K. Zhang, P.L. Marston, Acoustic radiation force expressed using complex phase shifts and momentum-transfer cross sections, J. Acoust. Soc. Am. 140 (2) (2016) El178–El183, http://dx.doi.org/10.1121/1.4959966.

[22] W. Wei, D.B. Thiessen, P.L. Marston, Acoustic radiation force on a compressible cylinder in a standing wave, J. Acoust. Soc. Am. 116 (1) (2004) 201–208, http://dx.doi.org/10.1121/1.1753291.

[23] P.L. Marston, W. Wei, D.B. Thiessen, Acoustic radiation force on elliptical cylinders and spheroidal objects in low frequency standing waves, AIP Conf. Proc. 838 (2006) 495–499, http://dx.doi.org/10.1063/1.2210403.

[24] Z.X. Gong, P.L. Marston, W. Li, T-matrix evaluation of three-dimensional acoustic radiation forces on nonspherical objects in bessel beams with arbitrary order and location, Phys. Rev. E 99 (6) (2019) 063004, http://dx.doi.org/10.1103/PhysRevE.99.063004.

[25] X.F. Zhang, G.B. Zhang, Acoustic radiation force of a Gaussian beam incident on spherical particles in water, Ultrasound Med. Biol. 38 (11) (2012) 2007–2017, http://dx.doi.org/10.1016/j.ultrasmedbio.2012.06.014.

[26] X.F. Zhang, Z.G. Song, D.M. Chen, G.B. Zhang, H. Cao, Finite series expansion of a Gaussian beam for the acoustic radiation force calculation of cylindrical particles in water, J. Acoust. Soc. Am. 137 (4) (2015) 1826–1833, http://dx.doi.org/10.1121/1.4916699.

[27] Y.P. Qiao, M.Y. Gong, H.B. Wang, J. Lan, T. Liu, J.H. Liu, Y.W. Mao, A.J. He, X.Z. Liu, Acoustic radiation force on a free elastic sphere in a viscous fluid: Theory and experiments, Phys. Fluids 33 (4) (2021) 047107, http://dx.doi.org/10.1063/5.0041249.

[28] Y.P. Qiao, H.B. Wang, X.Z. Liu, X.F. Zhang, Acoustic radiation force on an elastic cylinder in a Gaussian beam near an impedance boundary, Wave Motion 93 (2020) 102478, http://dx.doi.org/10.1016/j.wavemoti.2019.102478.

[29] Y.P. Qiao, X.W. Zhang, M.Y. Gong, H.B. Wang, X.Z. Liu, Acoustic radiation force and motion of a free cylinder in a viscous fluid with a boundary defined by a plane wave incident at an arbitrary angle, J. Appl. Phys. 128 (4) (2020) 044902, http://dx.doi.org/10.1063/5.0005866.

[30] H.B. Wang, S. Gao, Y.P. Qiao, J.H. Liu, X.Z. Liu, Theoretical study of acoustic radiation force and torque on a pair of polymer cylindrical particles in two Airy beams fields, Phys. Fluids 31 (4) (2019) 047103, http://dx.doi.org/10.1063/1.5088571.

[31] R.R. Wu, K.X. Cheng, X.Z. Liu, J.H. Liu, X.F. Gong, Y.F. Li, Study of axial acoustic radiation force on a sphere in a Gaussian quasi-standing field, Wave Motion 62 (2016) 63–74, http://dx.doi.org/10.1016/j.wavemoti.2015.12.005.

[32] A.K. Miri, F.G. Mitri, Acoustic radiation force on a spherical contrast agent shell near a vessel porous wall - theory, Ultrasound Med. Biol. 37 (2) (2011) 301–311, http://dx.doi.org/10.1016/j.ultrasmedbio.2010.11.006.

[33] F.G. Mitri, Acoustic radiation force acting on absorbing spherical shells, Wave Motion 43 (1) (2005) 12–19, http://dx.doi.org/10.1016/j.wavemoti.2005.05.001.

[34] F.G. Mitri, Acoustic radiation force acting on elastic and viscoelastic spherical shells placed in a plane standing wave field, Ultrasonics 43 (8) (2005) 681–691, http://dx.doi.org/10.1016/j.ultras.2005.03.002.

[35] F.G. Mitri, Acoustic radiation force on cylindrical shells in a plane standing wave, J. Phys. A: Math. Gen. 38 (42) (2005) 9395–9404, http://dx.doi.org/10.1088/0305-4470/38/42/016.

[36] F.G. Mitri, Frequency dependence of the acoustic radiation force acting on absorbing cylindrical shells, Ultrasonics 43 (4) (2005) 271–277, http://dx.doi.org/10.1016/j.ultras.2004.07.001.

[37] F.G. Mitri, Acoustic radiation force due to incident plane-progressive waves on coated cylindrical shells immersed in ideal compressible fluids, Wave Motion 43 (6) (2006) 445–457, http://dx.doi.org/10.1016/j.wavemoti.2006.02.005.

[38] F.G. Mitri, Calculation of the acoustic radiation force on coated spherical shells in progressive and standing plane waves, Ultrasonics 44 (3) (2006) 244–258, http://dx.doi.org/10.1016/j.ultras.2006.02.002.

[39] F.G. Mitri, Interaction of a high-order Bessel beam with a submerged spherical ultrasound contrast agent shell - Scattering theory, Ultrasonics 50 (3) (2010) 387–396, http://dx.doi.org/10.1016/j.ultras.2009.09.003.

[40] F.G. Mitri, Generalized theory of resonance excitation by sound scattering from an elastic spherical shell in a nonviscous fluid, IEEE Ultrason. Ferr. 59 (8) (2012) 1781–1790, http://dx.doi.org/10.1109/Tuffc.2012.2382.

[41] F.G. Mitri, Z.E.A. Fellah, Amplitude-modulated acoustic radiation force experienced by elastic and viscoelastic spherical shells in progressive waves, Ultrasonics 44 (3) (2006) 287–296, http://dx.doi.org/10.1016/j.ultras.2006.03.001.

[42] F.G. Mitri, T.P. Lobo, G.T. Silva, Axial acoustic radiation torque of a Bessel vortex beam on spherical shells, Phys. Rev. E 85 (2) (2012) 026602, http://dx.doi.org/10.1103/PhysRevE.85.026602.

[43] J.V. Venas, T. Jenserud, Exact 3D scattering solutions for spherical symmetric scatterers, J. Sound Vib. 440 (2019) 439–479, http://dx.doi.org/10.1016/j.jsv.2017.08.006.

[44] J.V. Venas, T. Jenserud, Generalization and stabilization of exact scattering solutions for spherical symmetric scatterers, J. Sound Vib. 539 (2022) 117263, http://dx.doi.org/10.1016/j.jsv.2022.117263.

[45] Z.Z. Chen, P.Z. Liu, X. Zhao, L. Huang, Y.X. Xiao, Y.H. Zhang, J.H. Zhang, N.J. Hao, Sharp-edge acoustic microfluidics: Principles, structures, and applications, Appl. Mater. Today 25 (2021) 101239, http://dx.doi.org/10.1016/j.apmt.2021.101239.

[46] X.Y. Ding, P. Li, S.C. S. Lin, Z.S. Stratton, N. Nama, F. Guo, D. Slotcavage, X.L. Mao, J.J. Shi, F. Costanzo, T.J. Huang, Surface acoustic wave microfluidics, Lab Chip 13 (18) (2013) 3626–3649, http://dx.doi.org/10.1039/c3lc50361e.

[47] Y. Gao, M.R. Wu, Y. Lin, J. Xu, Acoustic microfluidic separation techniques and bioapplications: A review, Micromachines 11 (10) (2020) 921, http://dx.doi.org/10.3390/mi11100921.

[48] L.Y. Yeo, J.R. Friend, Ultrafast microfluidics using surface acoustic waves, Biomicrofluidics 3 (1) (2009) 012002, http://dx.doi.org/10.1063/1.3056040.

[49] P.R. Zhang, H. Bachman, A. Ozcelik, T.J. Huang, Acoustic microfluidics, Annu. Rev. Anal. Chem. 13 (2020) 17–43, http://dx.doi.org/10.1146/annurev-anchem-090919-102205.

[50] P. Augustsson, T. Laurell, Acoustofluidics 11: Affinity specific extraction and sample decomplexing using continuous flow acoustophoresis, Lab Chip 12 (10) (2012) 1742–1752, http://dx.doi.org/10.1039/c2lc40200a.

[51] H. Bruus, Acoustofluidics 2: Perturbation theory and ultrasound resonance modes, Lab Chip 12 (1) (2012) 20–28, http://dx.doi.org/10.1039/c1lc20770a.

[52] H. Bruus, Acoustofluidics 10: Scaling laws in acoustophoresis, Lab Chip 12 (9) (2012) 1578–1586, http://dx.doi.org/10.1039/c2lc21261g.

[53] J. Dual, P. Hahn, I. Leibacher, D. Moller, T. Schwarz, J.T. Wang, Acoustofluidics 19: Ultrasonic microrobotics in cavities: devices and numerical simulation, Lab Chip 12 (20) (2012) 4010–4021, http://dx.doi.org/10.1039/c2lc40733g.

[54] M. Evander, J. Nilsson, Acoustofluidics 20: Applications in acoustic trapping, Lab Chip 12 (22) (2012) 4667–4676, http://dx.doi.org/10.1039/c2lc40999b.

[55] M. Gedge, M. Hill, Acoustofluidics 17: Theory and applications of surface acoustic wave devices for particle manipulation, Lab Chip 12 (17) (2012) 2998–3007, http://dx.doi.org/10.1039/c2lc40565b.

[56] P. Glynne-Jones, M. Hill, Acoustofluidics 23: acoustic manipulation combined with other force fields, Lab Chip 13 (6) (2013) 1003–1010, http://dx.doi.org/10.1039/c3lc41369a.

[57] S.S. Sadhal, Acoustofluidics 16: acoustics streaming near liquid-gas interfaces: drops and bubbles, Lab Chip 12 (16) (2012) 2771–2781, http://dx.doi.org/10.1039/c2lc40283a.

[58] S. Sepehrirahnama, A.R. Mohapatra, S. Oberst, Y.K. Chiang, D.A. Powell, K.M. Lim, Acoustofluidics 24: theory and experimental measurements of acoustic interaction force, Lab Chip 22 (18) (2022) 3290–3313, http://dx.doi.org/10.1039/d2lc00447j.

[59] Hossein Khodavirdi, Majid Rajabi, Sustainable pulling motion of an active scatterer, Wave Motion 119 (2023) 103134.

[60] Majid Rajabi, Hossein Khodavirdi, Alireza Mojahed, Acoustic steering of active spherical carriers, Ultrasonics 105 (2020) 106112.

[61] M. Rajabi, A. Hajiahmadi, Self-propulsive swimmers: Two linked acoustic radiating spheres, Phys. Rev. E 98 (6) (2018) 063003.

[62] Alireza Mojahed, Majid Rajabi, Self-motile swimmers: Ultrasound driven spherical model, Ultrasonics 86 (2018) 1–5.

[63] Majid Rajabi, Alireza Mojahed, Acoustic radiation force control: Pulsating spherical carriers, Ultrasonics 83 (2018) 146–156.

[64] Majid Rajabi, Alireza Mojahed, Acoustic manipulation of a liquid-filled spherical shell activated with an internal spherical oscillator, Acta Acust. united Acust. 103 (2) (2017) 210–218.
[65] M. Schoenberg, P.N. Sen, Properties of a periodically stratified acoustic half-space and its relation to a Biot fluid, J. Acoust. Soc. Am. 73 (1) (1983) 61–67, http://dx.doi.org/10.1121/1.388724.
[66] Y. Cheng, F. Yang, J.Y. Xu, X.J. Liu, A multilayer structured acoustic cloak with homogeneous isotropic materials, Appl. Phys. Lett. 92 (15) (2008) 151913, http://dx.doi.org/10.1063/1.2903500.
[67] S.A. Cummer, J. Christensen, A. Alù, Controlling sound with acoustic metamaterials, Nat. Rev. Mater. 1 (3) (2016) 16001, http://dx.doi.org/10.1038/natrevmats.2016.1.
[68] M.I. Hussein, M.J. Leamy, M. Ruzzene, Closure to "discussion of 'dynamics of phononic materials and structures: Historical origins, recent progress, and future outlook'", (Hussein, M.I., Leamy, M.J., and Ruzzene, M., 2014, ASME Appl. Mech. Rev., 66(4), p. 040802), Appl. Mech. Rev. 66 (4) (2014) 046002, http://dx.doi.org/10.1115/1.4027795.
[69] M. Kadic, T. Bückmann, R. Schittny, M. Wegener, Metamaterials beyond electromagnetism, Rep. Progr. Phys. 76 (12) (2013) 126501, http://dx.doi.org/10.1088/0034-4885/76/12/126501.
[70] M. Maldovan, Sound and heat revolutions in phononics, Nature 503 (7475) (2013) 209–217, http://dx.doi.org/10.1038/nature12608.
[71] S. Zhang, C.G. Xia, N. Fang, Broadband acoustic cloak for ultrasound waves, Phys. Rev. Lett. 106 (2) (2011) 024301, http://dx.doi.org/10.1103/PhysRevLett.106.024301.
[72] R. Abdulkadirov, P. Lyakhov, Estimates of mild solutions of Navier-Stokes equations in weak Herz-Type Besov-Morrey spaces, Mathematics 10 (5) (2022) 680, http://dx.doi.org/10.3390/math10050680.
[73] M.Y. Gong, Y.P. Qiao, J. Lan, X.Z. Liu, Far-field particle manipulation scheme based on X wave, Phys. Fluids 32 (11) (2020) 117104, http://dx.doi.org/10.1063/5.0027525.
[74] M.Y. Gong, Y.P. Qiao, Z.H. Fei, Y.Y. Li, J.H. Liu, Y.W. Mao, A.J. He, X.Z. Liu, Non-diffractive acoustic beams produce negative radiation force in certain regions, AIP Adv. 11 (6) (2021) 065029, http://dx.doi.org/10.1063/5.0056692.
[75] S. Deshmukh, Z. Brzozka, T. Laurell, P. Augustsson, Acoustic radiation forces at liquid interfaces impact the performance of acoustophoresis, Lab Chip 14 (17) (2014) 3394–3400, http://dx.doi.org/10.1039/c4lc00572d.
[76] M. Rajabi, A. Mojahed, Acoustic manipulation of oscillating spherical bodies: Emergence of axial negative acoustic radiation force, J. Sound Vib. 383 (2016) 265–276, http://dx.doi.org/10.1016/j.jsv.2016.06.042.
[77] Q. Wang, A. Riaud, J. Zhou, Z.X. Gong, M. Baudoin, Acoustic radiation force on small spheres due to transient acoustic fields, Phys. Rev. Appl. 15 (4) (2021) 044034, http://dx.doi.org/10.1103/PhysRevApplied.15.044034.
[78] H.Q. Yu, J. Yao, D.J. Wu, X.W. Wu, X.J. Liu, Negative acoustic radiation force induced on an elastic sphere by laser irradiation, Phys. Rev. E 98 (5) (2018) 053105, http://dx.doi.org/10.1103/PhysRevE.98.053105.